View metadata, citation and similar papers at core.ac.uk

brought to you by CORE

provided by Loughborough University Institutional Repository

This item was submitted to Loughborough's Institutional Repository (https://dspace.lboro.ac.uk/) by the author and is made available under the following Creative Commons Licence conditions.

creative commons

COMMONS DEED

Attribution-NonCommercial-NoDerivs 2.5

You are free:

- to copy, distribute, display, and perform the work

Under the following conditions:

Attribution. You must attribute the work in the manner specified by the author or licensor.

Noncommercial. You may not use this work for commercial purposes.

No Derivative Works. You may not alter, transform, or build upon this work.

- For any reuse or distribution, you must make clear to others the license terms of this work.
- Any of these conditions can be waived if you get permission from the copyright holder.

Your fair use and other rights are in no way affected by the above.

This is a human-readable summary of the Legal Code (the full license).

Disclaimer

For the full text of this licence, please go to:
http://creativecommons.org/licenses/by-nc-nd/2.5/

Depth-resolved whole-field displacement measurement using Wavelength Scanning Interferometry

Pablo D. Ruiz, Yanzhou Zhou, Jonathan M. Huntley and Ricky D. Wildman

Wolfson School of Mechanical and Manufacturing Engineering, Loughborough University, Ashby Road, Loughborough, Leicestershire. LE11 3TU, UK

e-mail: P.D.Ruiz@lboro.ac.uk - tel: 0044 1509 227592

Abstract

We describe a technique for measuring depth-resolved displacement fields within a 3-dimensional (3-D) scattering medium based on wavelength scanning interferometry. Sequences of 2-dimensional interferograms are recorded whilst the wavelength of the laser is tuned at constant rate. Fourier transformation of the resulting 3-D intensity distribution along the time axis reconstructs the scattering potential within the medium, and changes in the 3-D phase distribution measured between two separate scans provides one component of the 3-D displacement field. The technique is illustrated with a proof-of-principle experiment involving two independently controlled reflecting surfaces. Advantages over the corresponding method based on low coherence interferometry include a depth range unlimited by mechanical scanning devices, and immunity from fringe contrast reduction when imaging through dispersive media.

PACs codes: 42.25.Hz, 42.62.Eh, 42.87.Bg, 42.90.+m
Keywords: Depth-resolved, displacement measurements, Wavelength Scanning Interferometry, phase shifting, wavelength tuning.
Short title: Depth-resolved displacement measurement using Wavelength Scanning Interferometry.

1. Introduction

The ability to measure internal displacement fields within a material or structure would be highly desirable in many fields, ranging from alignment of complex optical systems to nondestructive evaluation of composites. Standard interferometric techniques (with either speckled or smooth wavefronts) have sufficient sensitivity for such applications but are typically restricted to the measurement of surface deformations. However, only in special cases is it possible to infer the internal deformation state of the structure or material from knowledge of the surface displacements alone.

Depth-discrimination with multiple wavelengths has been used in optical profilometry for a number of years. Two basic forms have been developed, depending on whether the multiple wavelengths are present simultaneously [1] or sequentially [2]. In the former case, denoted here by Low Coherence Interferometry (LCI), one illuminates with a broadband source and scans the reference mirror or sample through the required depth range. In the latter case, which we call Wavelength Scanning Interferometry (WSI), a tunable light source is used thereby avoiding the need for mechanical movement of the sample or the interferometer.

When measuring transparent objects (e.g, optical lenses or flats), reflections from surfaces beyond the surface of interest occur but are normally regarded as a nuisance, and wavelength tuning combined with specially-designed phase shifting algorithms have therefore been developed to suppress their effects [3,4]. Optical Coherence Tomography (OCT), on the other hand, is a rapidly developing imaging technology, primarily used for medical applications, that exploits the signal from subsurface reflections to provide information on the structure of biological tissues (see, for example, Ref. [5] for a recent review of the field). Most OCT systems operate in a pointwise manner, with mechanical scanning in one or more lateral directions to build up cross-sectional images, and are based on the LCI technique. The WSI version of OCT

was proposed by Fercher et al in 1995 [6], and demonstrated by a number of authors (see e.g. Ref. [7]).

The first demonstrations of depth-resolved displacement field measurement have been presented very recently [8][9]. These experiments were based on LCI: the interferometer is only sensitive to the movement of scattering points lying within the slice selected by the reference mirror position, and conventional fringe analysis algorithms can be used to extract the required displacement field.

The purpose of this paper is to present results from proof-of-principle experiments based on a WSI approach to sub-surface displacement field measurement. As far as we are aware, this is the first time that depth-resolved two-dimensional displacement fields have been demonstrated using wavelength scanning interferometry.

2. Wavelength Scanning Interferometry

For these proof-of-principle experiments we used the simplest possible sample configuration, shown in Fig. 1, consisting of two independently tiltable reflecting surfaces, S_1 and S_2. A third surface, R, provided the reference wave. All three surfaces were the glass-air interfaces of glass flats (thickness 5.1 mm), antireflection coated on one side to suppress the reflection from the second glass-air interface. The light source used was a solid-state tunable laser TL (New Focus Vortex 6005), the beam from which was expanded by lens L_1 and steered by mirror M towards collimating lens L_2. The reflected light from the three glass-air interfaces R, S_1 and S_2 was imaged by lens L_3 onto the sensor of a high-speed camera, C (VDS HCC-1000), which recorded the resulting 3-beam interference patterns.

The laser wavelength, λ, can be tuned in an approximately linear manner around a center wavelength, λ_c, by adjusting a voltage supplied by signal generator SG to the laser controller LC.

The time-varying phase difference $\phi(t) = 4\pi d/\lambda(t)$ between beams reflected back from any pair of surfaces can be expanded around λ_c in a first order Taylor series approximation as:

$$\phi(t) = \phi_0 + \frac{4\pi d}{\lambda_c} - \frac{4\pi d\Delta\lambda}{T{\lambda_c}^2}t \quad (1)$$

where ϕ_0 is the difference between the phase changes induced on reflection, d is the optical distance between the surfaces, $\Delta\lambda$ is the wavelength tuning range, T is the time it takes to scan through $\Delta\lambda$ and t is time ($-T/2 \le t \le T/2$). The second term on the right hand side of Eq. (1) is the phase due to the optical path difference between the surfaces. The third term is the phase shift introduced by tuning the wavelength and is equivalent to $2\pi ft$, where f is a carrier frequency proportional to d.

The intensity recorded at a particular pixel in the camera sensor, assuming that multiple reflections can be neglected, may be written as:

$$\begin{aligned} I(t) &= I_R + I_1 + I_2 + \\ &2\sqrt{I_R I_1}\cos[\phi_{R1}(t)] + 2\sqrt{I_R I_2}\cos[\phi_{R2}(t)] + 2\sqrt{I_1 I_2}\cos[\phi_{12}(t)] \end{aligned} \quad (2)$$

where I_R, I_1 and I_2 are the intensities of the beams coming from surfaces R, S_1 and S_2, respectively. ϕ_{R1}, ϕ_{R2}, ϕ_{12} are the phase differences between R and S_1, R and S_2 and S_1 and S_2, respectively, given by Eq.(1) and using the optical path differences d_{R1}, d_{R2}, d_{12} between the corresponding surfaces. A Fourier transform of $W(t)I(t)$, where W is a window function, then reveals (considering only positive frequencies) four amplitude peaks: the dc component and three peaks corresponding to each of the cosine terms, centered at frequencies f_{R1}, f_{R2} and f_{12}. Provided the distance between reference and sample is greater than the sample depth, the peaks of interest (f_{R1} and f_{R2}) are separated from the unwanted peaks (f_{12} and the dc), resulting in a reconstruction

of the true scattering potential of the sample, rather than the autocorrelation of the scattering potential [6].

The Fourier transform of $W(t)I(t)$ in the neighbourhood of the peak from surface j (j = 1, 2) may be written (neglecting constants and the contributions from other peaks) as

$$\tilde{I}(f) \otimes \tilde{W}(f) = \exp\left[i\phi_{Rj}(0)\right]\tilde{W}(f - f_{Rj}), \tag{3}$$

where ~ denotes Fourier transformed variables and $\otimes$ denotes convolution. The quantity $\phi_{Rj}(0)$, which is the phase at t = 0, i.e. at the centre wavelength λ_c, and which is related to the optical path between the surfaces, can therefore be retrieved by evaluating the arctangent of the ratio between the imaginary and real parts of $\tilde{I}(f_{Rj}) \otimes \tilde{W}(f_{Rj})$. If surface j is now displaced by an amount u_z in the out-of-plane direction, Eq. (1) shows that $\phi_{Rj}(0)$ changes by $4\pi u_z/\lambda_c$. The phase difference between $\phi_{Rj}(0)$ evaluated before and after displacement can therefore be used to calculate $u_z(x,y)$, where x and y are the two in-plane coordinates, provided that the phase of $\tilde{W}(f)$ is known and taken into account in the calculation.

The finite window duration has of course the effect of broadening a given spectral line. A rectangular window of duration T, for example, results in a sinc function of width (measured between the first zeros on either side of the maximum) $\Delta f = 2/T$. It can be shown that this corresponds to an effective depth resolution of $\delta = \lambda_c^2/\Delta\lambda$ (or a factor of 2 larger if using a Hanning window instead). Given that the coherence length of the laser is sufficient and that a Hanning window is used, it can be shown that the depth range (maximum distance a surface can be from the reference surface) is $\Delta z = \delta N_f/8$, where N_f is the number of frames acquired during time T while tuning the wavelength over the range $\Delta\lambda$. This is just a consequence of limiting the

carrier frequency *f* below one half the sampling rate of the camera in accordance with the Shannon sampling theorem.

One minor complication that should be pointed out is that the tilting of surface 1 will induce small phase shifts in the signal from surface 2, even if surface 2 does not itself move. This should be only a small effect in the current setup since the rate of change of phase with angle is zero for a plate initially oriented normal to the optical axis. This prediction is confirmed to be the case by the validation method presented in the next section. For more complex specimen geometries, however, it may be necessary when interpreting the phase change from any given layer to include the measured displacement information for all the preceding layers. Other factors that will also need to be considered when extending the technique to the measurement of true 3-D samples are the effect of multiple scattering, phase noise due to speckle decorrelation as the wavelength is tuned, and the development of a robust 3-D phase unwrapping algorithm [10].

3. Experimental results

The results presented here were obtained by tuning the laser wavelength around λ_c = 635.05nm at a rate $\Delta\lambda/T \sim 0.058\text{nm s}^{-1}$. A sequence of 940 interferograms was recorded with the camera running at 912 frames per second. The optical path difference between surfaces R and S_1 and S_1 and S_2 was approximately 51mm and 20mm, respectively.

Figure (2-a) shows the normalized intensity $I(t)$ measured for one pixel in the field of view, while Fig (2-b) shows the portion of the frequency spectrum of $I(t)$ where the peaks of interest are present. Prior to the Fourier transform, the mean value of the intensity signal was subtracted and the signal multiplied with a Hanning window. The peak frequencies for RS_1 and RS_2 are within 6% and 3%, respectively, from those expected using the third term of Eq. (1). The peak widths of approximately 4 Hz correspond to the expected value for a Hanning window of

$4/T$ where in this case $T \approx 1$ s. This corresponds to a depth resolution $\delta \approx 14$ mm. The depth range of the system was $\Delta z \approx 1650$ mm. Small independent tilts were then introduced to surfaces S_1 and S_2 and a second sequence of interferograms was recorded. Finally, the phase difference was obtained by subtracting the phase $\phi_{Rj}(0)$ evaluated for all the pixels in sequence 1 from the corresponding values in sequence 2.

Figures (3-a) and (3-b) show the measured wrapped phase difference maps for the movement of S_1 and S_2, respectively. The images show a region of about 10×10 mm^2 at a resolution of 256×256 pixels. Each fringe represents an out of plane displacement $u_z = \lambda_c/2 \sim 317$ nm. Figure 4 shows the displacement field obtained for S_1 and S_2 after unwrapping the phase difference maps shown in Fig. 3. The original spatial resolution of 256×256 pixels has been reduced by a factor of ten along each axis for clarity in the mesh plot.

In order to validate the results, the tilts were measured independently using standard two-beam interferometry at a fixed wavelength between surfaces R-S_1 and R-S_2. Only one of the two sample surfaces (S_1 and S_2) was present at a time. The optical phase difference was evaluated for each case using a spatial phase shifting method [11]. Figure 5 shows four profiles corresponding to the displacements measured for S_1 and S_2 at x = 5mm with WSI and with two beam interferometry.

The tilt angles about the x and y axes were calculated as Ω_x = 21 μrad and Ω_y = 306 μrad for surface S_1, and Ω_x = 112 μrad and Ω_y = 48 μrad for surface S_2. The discrepancies between the tilt angles measured with both methods for the horizontal, x, and vertical, y, directions were e_{1x}= 0.9, e_{1y}= 5.0 μrad for surface S_1 and e_{2x}= 1.9, e_{2y}= 1.0 μrad for S_2. Although this can be regarded as good agreement, a small phase offset error was found between the two methods, as can be seen in Fig. 5, and may be attributed to drifts in λ_c between successive recording

sequences.. In some applications a constant phase offset may not be an issue, but in situations where it is important to measure absolute displacements the problem could be overcome by incorporating a reference etalon into the interferometer.

4. Discussion

The results presented in the previous section suggest that WSI is a viable technique for depth-resolved displacement field measurement. In this section we discuss its strengths and weaknesses compared to the LCI version [8][9].

The main disadvantage is that images need to be acquired for all wavelengths before even a single slice can be selected. The use of a 1 kHz framing camera on this demonstration system nevertheless allowed all data acquisition to be performed in ~1 s, a figure which is compatible with high-volume production testing.

On the other hand we can foresee at least three significant advantages, which are summarized here. Firstly, the depth range of the displacement field is limited only by the coherence length of the laser, rather than by the mechanical scan range of the reference arm of the interferometer as in Low Coherence Interferometry. There seems no reason why depth ranges that would be regarded as unfeasible for LCI (of order 1 m or more) cannot be measured using WSI. Secondly in systems with broadband light sources, dispersion may be a significant cause of fringe contrast reduction. In WSI the fringes are produced at high visibility at all times by a single wavelength and therefore the reduction in data quality due to dispersion does not arise. Finally, the limited dynamic range of wholefield image sensors based on CCD or CMOS technology (the number of grey levels, N_g, is typically only 256) limits the performance of WSI to a much lesser extent than that of LCI. If δ is the slice thickness and Z the overall thickness of a sample containing uniformly distributed scatterers, then only the fraction δ/Z of scattered

photons contribute interferometric signal in the case of LCI, the rest merely producing a dc offset to the intensity image. The modulation depth can therefore never exceed $N_g\delta/Z$ grey levels, and as a result, attempts to improve the axial resolution (i.e. reduce δ) have the unfortunate consequence of reducing the intensity modulation by a corresponding factor. For example, in the case $\delta/Z = 1/100$, with an 8-bit camera, the signal would be no more than 2-3 grey levels deep and the measurements therefore rather susceptible to noise. WSI on the other hand ensures that the full dynamic range of the camera is utilized, and may be expected to have a signal to noise ratio some (Z/δ) times greater than with LCI.

5. Conclusions

We have demonstrated how Wavelength Scanning Interferometry can be used to measure depth-resolved displacement fields of different surfaces through transparent media. The depth resolution is limited by the wavelength tuning range and the number of frames registered by the camera whilst the wavelength is tuned. Like the Low-Coherence Interferometry (LCI) version, the method provides decoupling of the depth resolution and displacement sensitivity. However, our approach has a number of potential benefits over LCI, in particular the avoidance of mechanical scanning (particularly important for large specimens) and the ability to make measurements even in the presence of significant optical dispersion and image sensors with low dynamic range.

6. References

[1] T. Dresel, G. Hausler and H. Venzke, "3-dimensional sensing of rough surfaces by coherence radar," *Appl. Opt.* **31,** 919-925 (1992).

[2] S. Kuwamura and I. Yamaguchi, "Wavelength scanning profilometry for real-time surface shape measurement", *Appl. Opt.* **36,** 4473-4482 (1997).

[3] P. de Groot, "Measurement of transparent plates with wavelength-tuned phase-shifting interferometry", *Appl. Opt.* **39,** 2658-2663 (2000).

[4] K. Hibino, B. F. Oreb, P. S. Fairman and J Burke, "Simultaneous measurement of surface shape and variation in optical thickness of a transparent parallel plate in wavelength-scanning Fizeau interferometer" *Appl. Opt.* **43** (6) 1241-1249 (2004).

[5] F. Fercher, W. Drexler, C. K. Hitzenberger, and T. Lasser, "Optical coherence tomography - principles and applications", *Rep. Prog. Phys.* **66,** 239-303 (2003).

[6] F. Fercher, C. K. Hitzenberger, G. Kamp and S. Y. El-Zaiat, "Measurement of intraocular distances by backscattering spectral interferometry", *Opt. Comm.* **117,** 43-48 (1995).

[7] F. Lexer, C. K.Hitzenberger, A. F. Fercher, and M. Kulhavy, "Wavelength-tuning interferometry of intraocular distances," *Appl. Opt.* **36,** 6548-6553 (1997).

[8] G. Gülker, K. D. Hinsch, A. Kraft, "Low-coherence ESPI in the investigation of ancient terracotta warriors", in *Proc SPIE Speckle Metrology 2003* **4933,** Kay Gastinger, Ole J. Løkberg, Svein Winther; Eds.(Trondheim, Norway, 2003), pp. 53-58

[9] K. Gastinger, S. Winther, K. D. Hinsch "Low-coherence speckle interferometer (LCSI) for characterization of adhesion in adhesive-bonded joints", in *Proc SPIE Speckle Metrology 2003* **4933,** Kay Gastinger, Ole J. Løkberg, Svein Winther; Eds.(Trondheim, Norway, 2003) , pp. 59-65

[10] J.M. Huntley, "Three-dimensional noise-immune phase unwrapping algorithm", *Appl. Opt.* **40** 3901-3908 (2001).

[11] M. Takeda, H. Ina and S. Kobayashi, “Fourier-transform method of fringe-pattern analysis for computer-based topography and interferometry”, *JOSA* **72**, 156-160 (1982).

7. Figure captions

Figure 1. Optical setup showing tunable laser (TL), signal generator (SG), laser controller (LC), lenses (L_1, L_2, L_3), steering mirror (M), reference surface (R), surfaces under test (S_1, S_2), high-speed camera (C) and personal computer (PC).

Figure 2. (a) Normalized intensity signal recorded at one pixel with the high-speed camera. (b) Frequency spectrum of Fig. 2(a). The peaks RS_1, RS_2 and S_1S_2 correspond to the interference signal for surfaces R and S_1, R and S_2 and S_1 and S_2, respectively.

Figure 3. Wrapped phase difference map of S_1 (a) and S_2 (b) showing the tilt introduced for each surface. Black represents $-\pi$ radians and white $+\pi$ radians.

Figure 4. Displacement due to independent tilt of surfaces S_1 and S_2 measured simultaneously using WSI.

Figure 5. Comparison of the displacements measured independently with WSI and with standard two beam interferometry for surfaces S_1 and S_2 at x = 5mm.

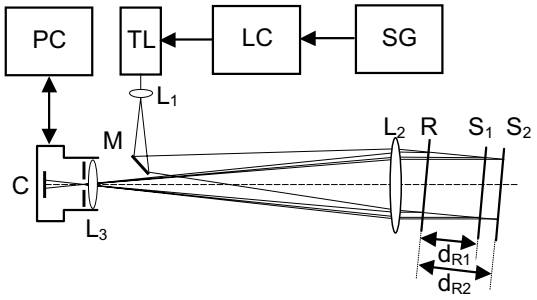

Figure 1. Optical setup showing tunable laser (TL), signal generator (SG), laser controller (LC), lenses (L1, L2, L3), steering mirror (M), reference surface (R), surfaces under test (S1, S2), high-speed camera (C) and personal computer (PC).

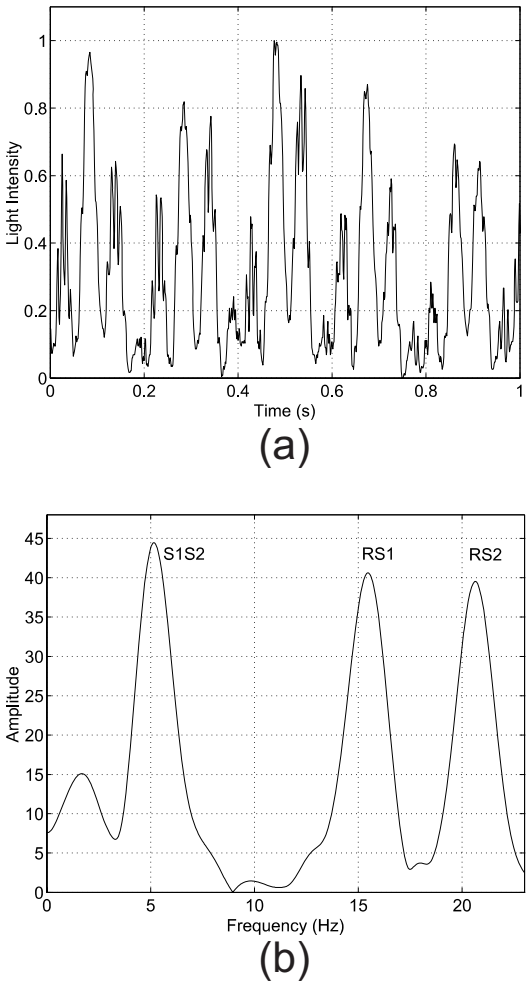

Figure 2. (a) Normalized intensity signal recorded at one pixel with the high-speed camera. (b) Frequency spectrum of Fig. 2(a). The peaks RS1, RS2 and S1S2 correspond to the interference signal for surfaces R and S1, R and S2 and S1 and S2, respectively.

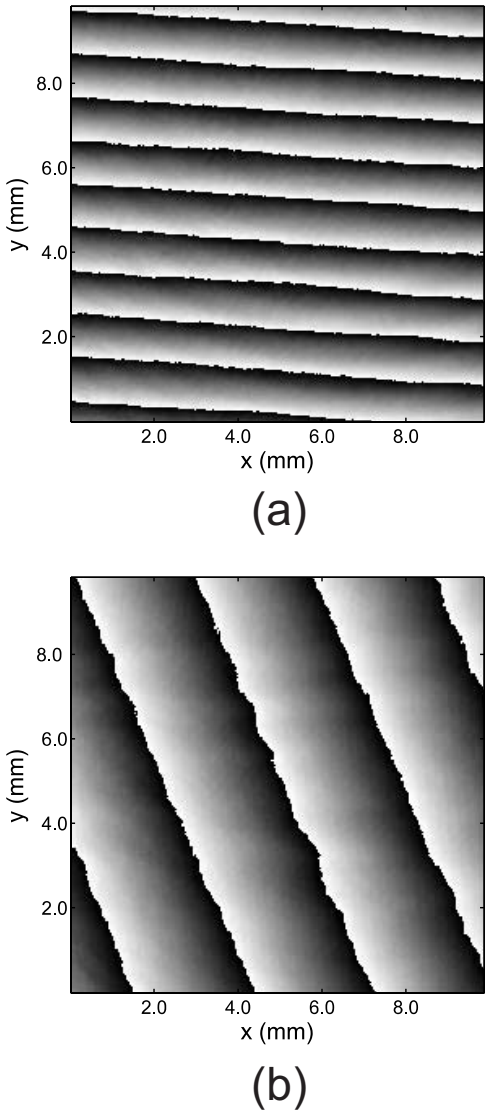

Figure 3. Wrapped phase difference map of S_1 (a) and S_2 (b) showing the tilt introduced for each surface. Black represents -π radians and white +π radians.

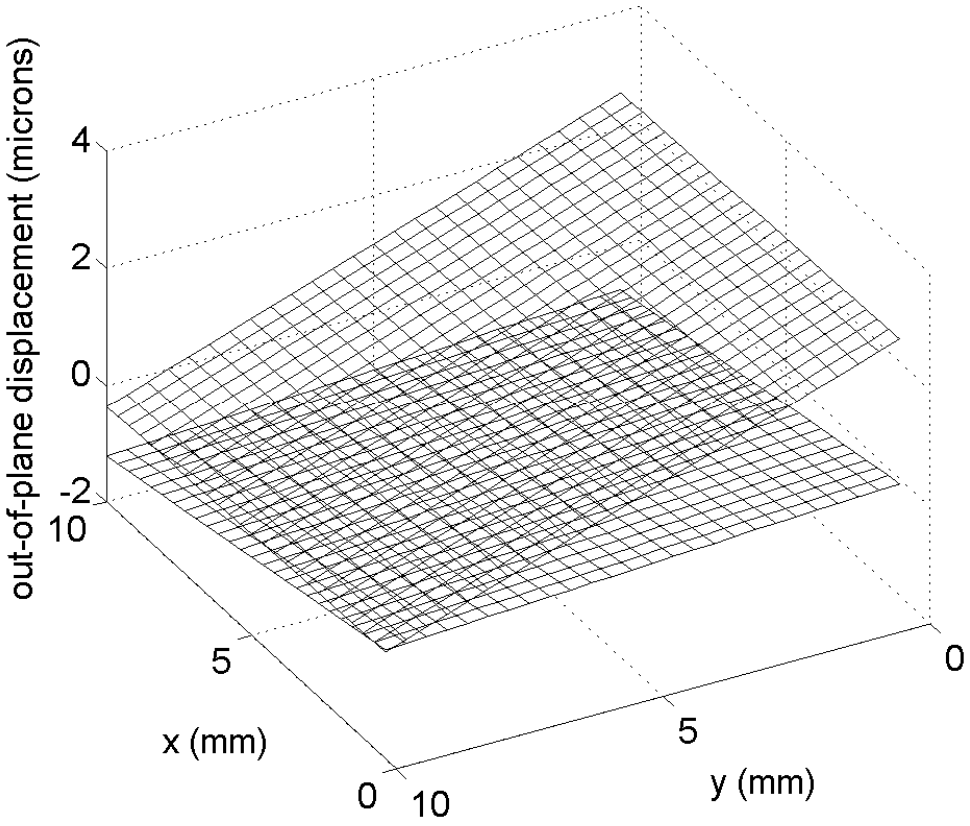

Figure 4. Displacement due to independent tilt of surfaces S_1 and S_2 measured simultaneously using WSI.

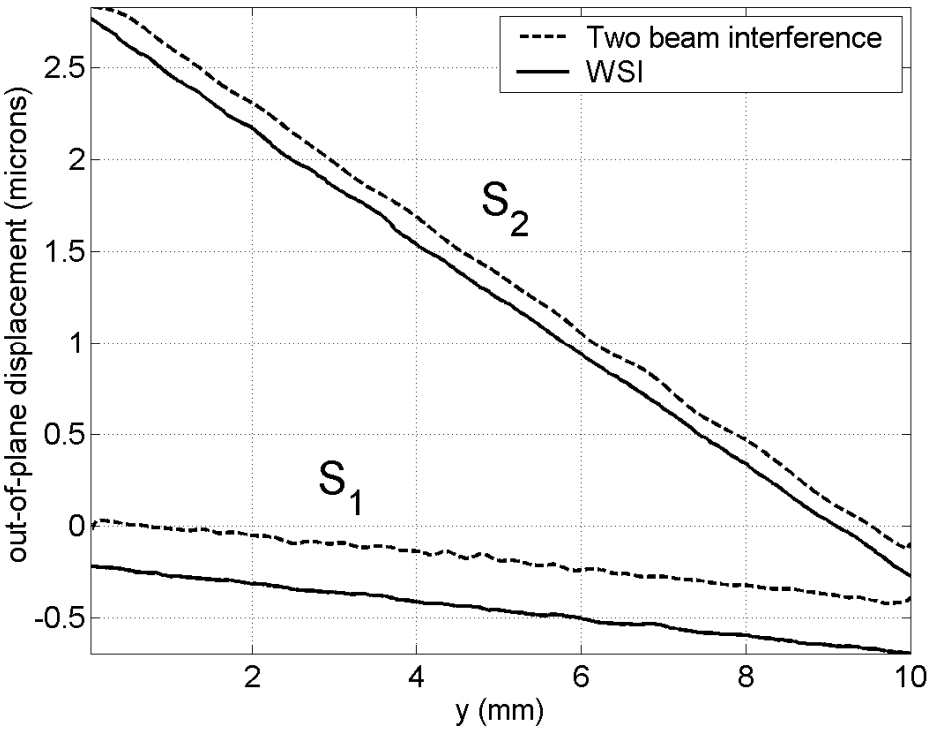

Fig. 5 Comparison of the displacements measured independently with WSI and with standard two beam interferometry for surfaces S_1 and S_2 at x = 5mm